HAL open science

A New Land Cover Map of Two Watersheds under Long-Term Environmental Monitoring in the Swedish Arctic Using Sentinel-2 Data

Yves Auda, Erik J Lundin, Jonas Gustafsson, Oleg S Pokrovsky, Simon Cazaurang, Laurent Orgogozo

To cite this version:

Yves Auda, Erik J Lundin, Jonas Gustafsson, Oleg S Pokrovsky, Simon Cazaurang, et al.. A New Land Cover Map of Two Watersheds under Long-Term Environmental Monitoring in the Swedish Arctic Using Sentinel-2 Data. Water, 2023, 15 (18), pp.3311. 10.3390/w15183311 . hal-04290497

HAL Id: hal-04290497

https://hal.science/hal-04290497v1

Submitted on 16 Nov 2023

HAL is a multi-disciplinary open access archive for the deposit and dissemination of scientific research documents, whether they are published or not. The documents may come from teaching and research institutions in France or abroad, or from public or private research centers.

L'archive ouverte pluridisciplinaire **HAL**, est destinée au dépôt et à la diffusion de documents scientifiques de niveau recherche, publiés ou non, émanant des établissements d'enseignement et de recherche français ou étrangers, des laboratoires publics ou privés.

Public Domain

water

MDPI

Article

A New Land Cover Map of Two Watersheds under Long-Term Environmental Monitoring in the Swedish Arctic Using Sentinel-2 Data

Yves Auda [1,*], Erik J. Lundin [2], Jonas Gustafsson [2], Oleg S. Pokrovsky [1,3], Simon Cazaurang [4] and Laurent Orgogozo [1]

1 GET (Géosciences Environnement Toulouse), UMR 5563 CNRS/UR 234 IRD/UPS, Observatoire Midi Pyrénées, Université de Toulouse, 31400 Toulouse, France; oleg.pokrovski@get.omp.eu (O.S.P.); laurent.orgogozo@get.omp.eu (L.O.)
2 Swedish Polar Research Secretariat, Abisko Scientific Research Station, SE-971 87 Luleå, Sweden; erik.lundin@polar.se (E.J.L.); volehunter@gmail.com (J.G.)
3 BIO-GEO-CLIM Laboratory, Tomsk State University, 634050 Tomsk, Russia
4 Toulouse Institute of Fluid Mechanics (IMFT), National Polytechnic Institute of Toulouse, 31400 Toulouse, France; simon.cazaurang@imft.fr
* Correspondence: yves.auda@get.omp.eu

Abstract: A land cover map of two arctic catchments near the Abisko Scientific Research Station was obtained based on a classification from a Sentinel-2 satellite image and a ground survey performed in July 2022. The two contiguous catchments, Miellajokka and Stordalen, are covered by various ecotypes, from boreal forest to alpine tundra and peatland. Two classification algorithms, support vector machine and random forest, were tested and gave very similar results. The percentage of correctly classified pixels was over 88% in both cases. The developed workflow relies solely on open-source software and acquired ground observations. Space organization was directed by the altitude as demonstrated by the intersection of the land cover with the topography. Comparison between this new land cover map and previous ones based on data acquired between 2008 and 2011 shows some trends in vegetation cover evolution in response to climate change in the considered area. This land cover map is key input data for permafrost modeling and, hence, for the quantification of climate change impacts in the studied area.

Keywords: land cover; Sentinel-2 images; support vector machine; random forests; boreal forest; alpine tundra

check for updates

Citation: Auda, Y.; Lundin, E.J.; Gustafsson, J.; Pokrovsky, O.S.; Cazaurang, S.; Orgogozo, L. A New Land Cover Map of Two Watersheds under Long-Term Environmental Monitoring in the Swedish Arctic Using Sentinel-2 Data. *Water* **2023**, *15*, 3311. https://doi.org/10.3390/w15183311

Academic Editor: Alexander Shiklomanov

Received: 24 August 2023
Revised: 15 September 2023
Accepted: 16 September 2023
Published: 19 September 2023

Copyright: © 2023 by the authors. Licensee MDPI, Basel, Switzerland. This article is an open access article distributed under the terms and conditions of the Creative Commons Attribution (CC BY) license (https://creativecommons.org/licenses/by/4.0/).

1. Introduction

The nature of the land cover, including vegetation covers, bare rock outcrops, and surface water bodies, is of major importance to understanding hydrological and biogeochemical fluxes on continental surfaces [1–3]. It is especially true in the Arctic, where permafrost conditions exert controls on the present ecotypes and their distributions [4–7], while vegetation cover variability may, in turn, strongly impact thermo-hydrological conditions [8,9]. In permafrost-affected soils, strong coupling between water and heat transfer occurs, and thus, the thermal buffering of the vegetation cover is a key determinant of permafrost dynamics [10–14]. Evapotranspiration fluxes may also be a dominant term of the water budget in permafrost regions [15,16]. For all these reasons, permafrost modeling requires detailed knowledge of up-to-date land cover distribution.

The vast extension and the remoteness of the Arctic regions make the establishment of field survey-based land cover maps difficult. Moreover, fine resolutions and open data maps are needed for many applications [17], including permafrost modeling. Thus, there is a growing interest in airborne [18,19] and remote sensing [20–22] observations capable of producing fine resolution vegetation maps in the Arctics. These regions are experiencing

intensive climate change [23]. Permafrost thawing results in methane and carbon dioxide emissions [24], which contribute to the greenhouse effect. These modifications induce changes in ecotypes [25] visible at the landscape level. Thus, there is a need for not only fine spatial resolution maps but also for fine temporal resolution surveys. In order to produce regularly updated land cover maps for large areas, the use of remote sensing data from long-term satellite missions combined with in situ information is required [21].

Here, we present a workflow for creating fine-resolution vegetation maps using only open data and open-source software along with dedicated field data. The workflow is applied to two watersheds in the Swedish Arctic, for parts of which previous vegetation maps at coarser resolutions and/or in past climatic conditions were already available [18,26,27]. The obtained map is used for investigating a link between topography and vegetation distribution and assessing the temporal evolution of the vegetation cover during a 14-year period (2008–2022). This information is crucially important for future permafrost modeling studies of the studied sites to be conducted with the cryohydrogeological simulator permaFoam [16,28], and it will also provide new insights into contemporary landscape evolution in this type of environment.

2. Materials and Methods

2.1. General Geographic Information about the Study Area

Two watersheds close to Abisko Scientific Research Station (INTERACT Network) were studied (Figure 1). The first one, from West to East, is Miellajokka, a sub-alpine catchment that includes the iconic mounts of Tjuonavagge. This 51.5 km^2 catchment presents altitudes ranging from 383 to 1731 m above sea level [29]. The most eastern watershed is Stordalen, a 16 km^2 catchment with a lake-rich, peat-rich Northern part and a sub-alpine Southern part, with elevation between 350 and 770 m above sea level [30–33]. In Stordalen, vegetation maps of the Northern, low-elevation part have already been produced based on airborne data from 2000 [26]. Later on, another vegetation map for the whole watershed was produced using airborne data from 2008 [27]. Both Stordalen and Miellajokka are encompassed in the area studied by Reese et al. [18], with a vegetation map established on the basis of 2010 satellite images also using data acquired by a lidar survey.

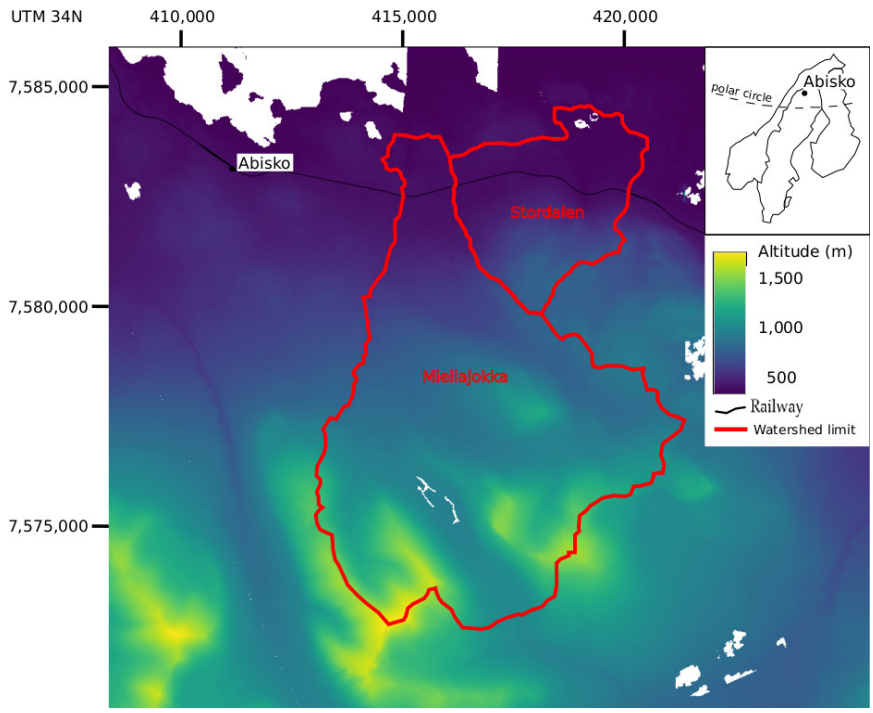

Figure 1. Location of the study zone on the articDEM map.

2.2. Satellite Image and Digital Elevation Model

Obtaining images in the Arctic zone to study vegetation cover is difficult. These geographical areas are covered with snow for a large part of the year, which prevents any satellite study of the vegetation cover. In addition, frequent clouds hinder the acquisition of optical images. A single Sentinel-2 image acquired on 25 August 2022 was downloaded from https://peps.cnes.fr (accessed on 18 September 2023). Ten bands were selected for land cover classification ($B02$—blue, $B03$—green, $B04$—red, $B05$—red-edge, $B06$—red-edge, $B07$—red-edge, $B08$—NIR, $B08A$—narrow NIR, $B11$—SWIR 1, $B12$—SWIR 2). The image is not corrected for atmospheric effects (Level-1C). The images are stored in the UTM34N reference coordinate system, and all calculations are performed in this system to avoid altering the radiometry by re-projection.

On the basis of four ($B03$, $B04$, $B08$, $B11$) out of the 10 acquired channels, four derived indicators were calculated: Bright, NDVI, NDWI, and NDII (Table 1). The bright index is very sensitive to albedo. It distinguishes between light and dark soils. The NDWI (Normalized Difference Water Index) was used to detect water areas. The NDVI (Normalized Difference Vegetation Index) expressed the photosynthesis of the vegetation cover. The use of NDII (Normalized Difference Infrared Index) [34,35] did not improve the results and was not retained for the final classification.

Table 1. Vegetation indicators. Band notation corresponds to the MSI sensor of the Sentinel-2 satellite.

Index	Formula
Bright	$\sqrt{(B04 * B04)/(B08 * B08)}$
NDVI	$(B08 - B04)/(B08 + B04)$
NDWI	$(B03 - B08)/(B03 + B08)$
NDII	$(B08 - B11)/(B08 + B11)$

Since vegetation in mountainous areas is related to altitude, the digital terrain model is a very useful data source. ArcticDEM is an NGA-NSF public–private initiative to automatically produce a fine-resolution digital surface model of the Arctic using optical stereo imagery. The majority of ArcticDEM data were generated from the panchromatic bands of the WorldView-1, WorldView-2, and WorldView-3 satellites and, for a small percentage of data, from the GeoEye-1 satellite. For this study, ArticDEM Release 7 "mosaic" format files with a spatial resolution of 2 m were downloaded at https://data.pgc.umn.edu/elev/dem/setsm/ArcticDEM/mosaic/v3.0/ (accessed on 18 September 2023).

2.3. Field Survey

The ground-truth survey took place from 21 July 2022 to 24 July 2022 in the Miellajokka and Stordalen watersheds in northern Sweden. We geolocalized areas of the different land cover types in the field using GPS, GLONASS, Beidou, and Galileo navigation systems supported by a Samsung Galaxy Tab S6 Lite tablet. The Qfield software was used for data entry in the field. Its compatibility with QGIS simplifies data collection and subsequent analysis [36].

Prior to the field survey, a database including a color composite of Sentinel-2 image channels B08/B04/B03, the Open Street Map data, and a vector layer with no record was prepared in QGIS and then transferred to Qfield.

Areas of observed and land cover types were highlighted as polygons in Figure 2. Each polygon served a ground truth location established by direct observation during the field survey of an area covered by a clearly identified land cover class. As a complement, a photo of the most characteristic observations was taken with the tablet camera.

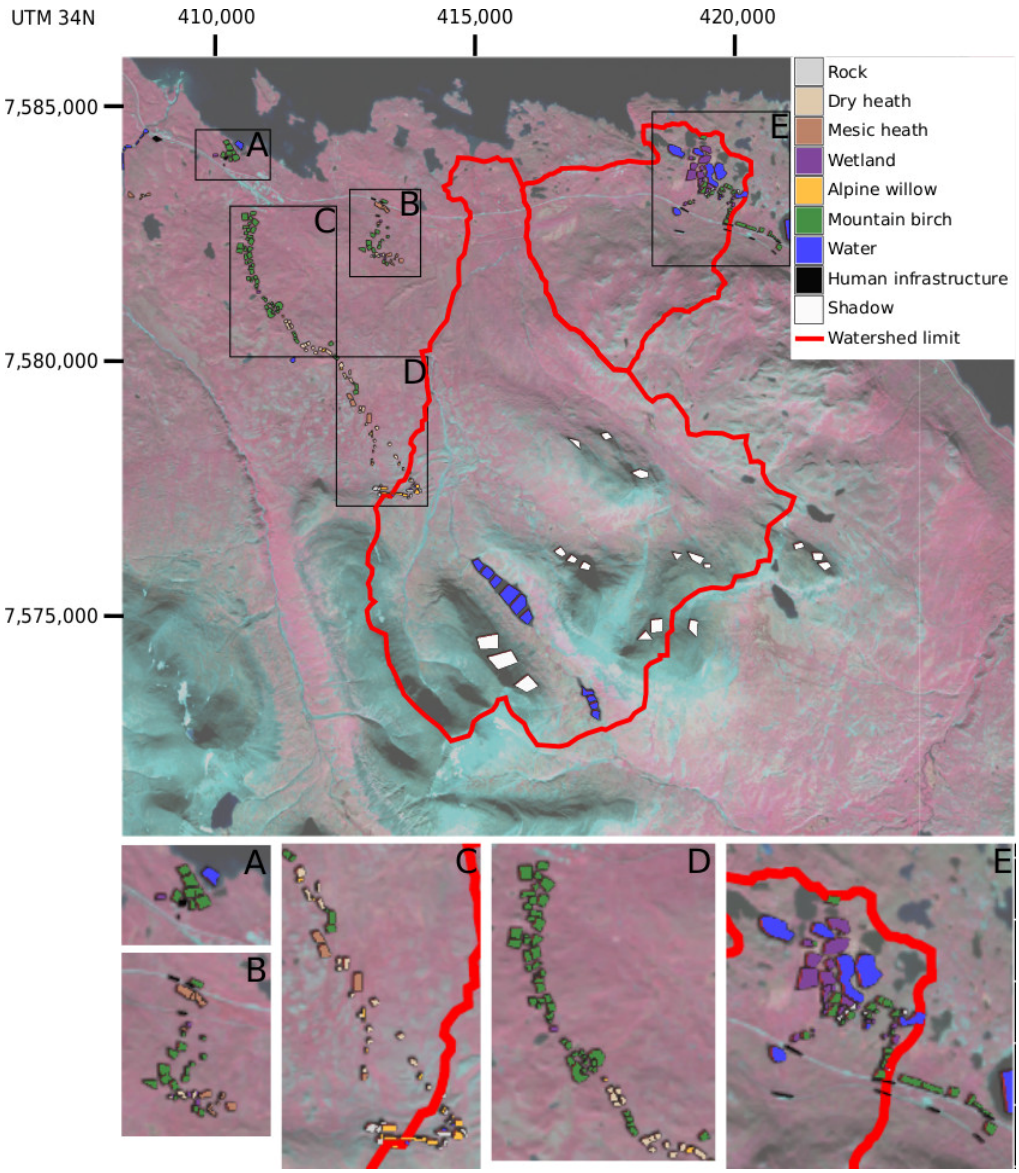

Figure 2. Field survey drawn on color composites of Sentinel-2 images channels *B*08, *B*04, *B*03. (**A**–**E**): zoom in on field survey zones.

The 270 observations conducted during the field survey only identified seven out of the 12 classes by Reese et al. [18]. "Alpine meadow" was not encountered enough to constitute an individual class. Likewise, the "Mountain birch–meadow" class was only observed in six ground truth polygons and was grouped with the "Mountain birch–moss" class to form a single "Mountain birch" class. Snowbeds were poorly represented and were not included. "Grass heaths" were not encountered. Further, the "Rock" class mainly represents bedrock outcrops but may also include thin organic soil and sediment. "Human infrastructure" was added as a new class, mainly representing the road and the railway passing through the mapped area. Shadows in the steep areas to the south of the study area hinder recognition of the landscape they cover. To avoid confusion, especially with water, a "Shadow" class was created, summarizing the total number of classes to nine (Table 2).

As far as possible, the number of survey polygons was balanced between the representative classes. Poor accessibility due to difficult terrain limited the choices of locations (Figure 2). Thus, a randomized field survey design was not possible in this natural environment. The transition from one land-use class to another is sometimes gradual, making it

difficult to assign an area to a specific class. For this reason, surveys were only carried out in areas that are homogeneous in terms of the characteristics of the land cover classes.

Table 2. Land cover classes.

Class	Number of Polygons	Number of Pixels
Rock	25	361
Dry heath	35	889
Mesic heath	21	801
Wetland	29	1614
Alpine willow	19	402
Mountain birch	105	4587
Water	30	8568
Human infrastructure	13	312
Shadow	18	7026

2.4. Classification

There are multiple machine learning algorithms used to create land cover classification maps from satellite images. Two supervised learning algorithms, support vector machine (SVM) and random forest (RF), have become prominent in recent years [37]. SVM achieves a higher level of classification accuracy and can be used with small training data sets and high-dimension data [38,39]. Its principle is based on the creation of hyperplanes to separate objects according to their class. RF is widely used in image classification studies [40,41]. It uses decision trees and random draws of samples and variables to classify the Sentinel-2 image. These data were analyzed successively with SVM and RF. Within each class, 30% of the surveyed polygons were randomly drawn and reserved for classification quality assessment. The classification was trained with the remaining 70%. GRASS software was used for the calculations [42]. The extension r.learn.ml2 interfaces with the Scikit-learn library written in Python to perform classifications.

3. Results

3.1. Vegetation Map in Current Climatic Conditions

The statistics computed from surveyed polygons reserved for classification quality assessment confirm the quality of the classifications. The percentage of pixels correctly classified by SVM is 92%, while it is 88% by RF. The confusion matrices (Tables 3 and 4) provide an analysis of the accuracy of the classification used for building our map at the class level. The two classifications are very close. If the shadow class is not taken into account, the percentages of pixels correctly classified become 89% for SVM and 88% for RF. SVM is chosen for further analysis because confusion between "Alpine willow" and "Moutain birsh" is less important for this algorithm.

The confusion between "Dry heath" and "Mesic heath" is understandable because these two formations are differentiated primarily by canopy height, a feature not accessible from the images used in our study. Likewise, the confusion between "Alpine willow" and "Wetland" is due to the difficulty of recognizing spaces occupied by a few willow plants. In addition, with such a pixel classification approach, places that are temporarily flooded at the moment of the satellite image acquisition are difficult to distinguish from true wetlands, i.e., places under water almost all along the active season. This could lead to an overestimation of the wetland area since places with other vegetation types, such as meadows, may be temporarily flooded with groundwater discharge or snowmelt water. Another important point is the detection of temporary high-elevation open water bodies in several places around Tjuonavagge Lake, according to both this classification and the two indicator values, NDII and NDVI, of the pixels. These ones may be generated by late snow

melt in the highest places of the landscape. Finally, the confusion between "Dry heath," "Mesic heath," and "Mountain birch" may be related to the fact that these classes can be contiguous and even associated in some places. It describes mixed spaces where several classes coexist, i.e., ecotone between these classes.

Table 3. Confusion matrix of the support vector machine classification. The asterisks (*) in the confusion matrix indicate the most important confusions. The columns show the field surveys, and the rows show the classification results. For instance, the number 130 corresponds at the cross of the "Mountain birch" line, and the "Mesic heath" column means that 130 pixels that have been classified as "Mountain birch" belong to "Mesic heath" according to the field survey.

	Rock	**Dry Heath**	**Mesic Heath**	**Wetland**	**Alpine Willow**	**Mountain Birch**	**Water**	**Human Infrastructure**	**Shadow**
Rock	87	11	22	0	2	2	0	1	0
Dry heath	0	140	48 *	1	14	0	0	0	0
Mesic heath	17	27	38	0	2	5	0	0	0
Wetland	0	2	6	550	34 *	11	9	0	0
Alpine willow	0	7	0	6	87	5	0	0	0
Mountain birch	0	101 *	130 *	46 *	14	1307	7	0	0
Water	0	0	0	0	0	0	2914	17	25
Human infrastructure	1	0	0	0	0	0	8	46	0
Shadow	4	0	0	0	0	0	39 *	10	2335

Table 4. Confusion matrix of the random forests classification. The asterisks (*) in the confusion matrix indicate the most important confusions. The columns show the field surveys, and the rows show the classification results. For instance, the number 117 corresponds at the cross of the "Mountain birch" line, and the "Mesic heath" column means that 117 pixels that have been classified as "Mountain birch" belong to "Mesic heath" according to the field survey.

	Rock	**Dry Heath**	**Mesic Heath**	**Wetland**	**Alpine Willow**	**Mountain Birch**	**Water**	**Human Infrastructure**	**Shadow**
Rock	84	2	15	0	0	1	0	3	0
Dry heath	0	168	59 *	11	18	2	0	0	0
Mesic heath	17	18	49	5	6	8	0	0	0
Wetland	0	0	0	484	51 *	6	4	1	0
Alpine willow	0	2	4	0	40	1	0	0	0
Mountain birch	0	98*	117 *	102 *	38 *	1312	8	1	0
Water	2	0	0	1	0	0	2913	12	309
Human infrastructure	1	0	0	0	0	0	8	47	0
Shadow	5	0	0	0	0	0	44 *	10	2051

All the pixels classified as "Alpine willow" belong to this class. An area classified as "Alpine willow" therefore corresponds to this class. However, an area covered by this class is not always assigned to it. Thus, the area classified as "Alpine willow" is underestimated. Furthermore, 22% of the pixels in the confusion matrix classified as "Mountain birch" do not belong to this class. An area covered by this class is always assigned to this class. The area classified as "Mountain birch," which occupies more than 40% of the space, is therefore overestimated. (Table 5). The "Rock" class and the wetlands ("Wetland" and "Alpine willow") share 40% of the spaces. The other classes are much smaller.

Table 5. Distribution of land cover classes of our classification. The shadow class is not taken into account.

Class	Percentage
Rock	38
Dry heath	12
Mesic heath	4
Wetland	16
Alpine willow	7
Mountain birch	14
Water	6
Human infrastructure	1

The classified image (Figure 3) shows patterns consistent with the knowledge of the terrain. The transport infrastructure is described with precision in its continuity. Lake Torneträsk in the north is homogeneously identified.

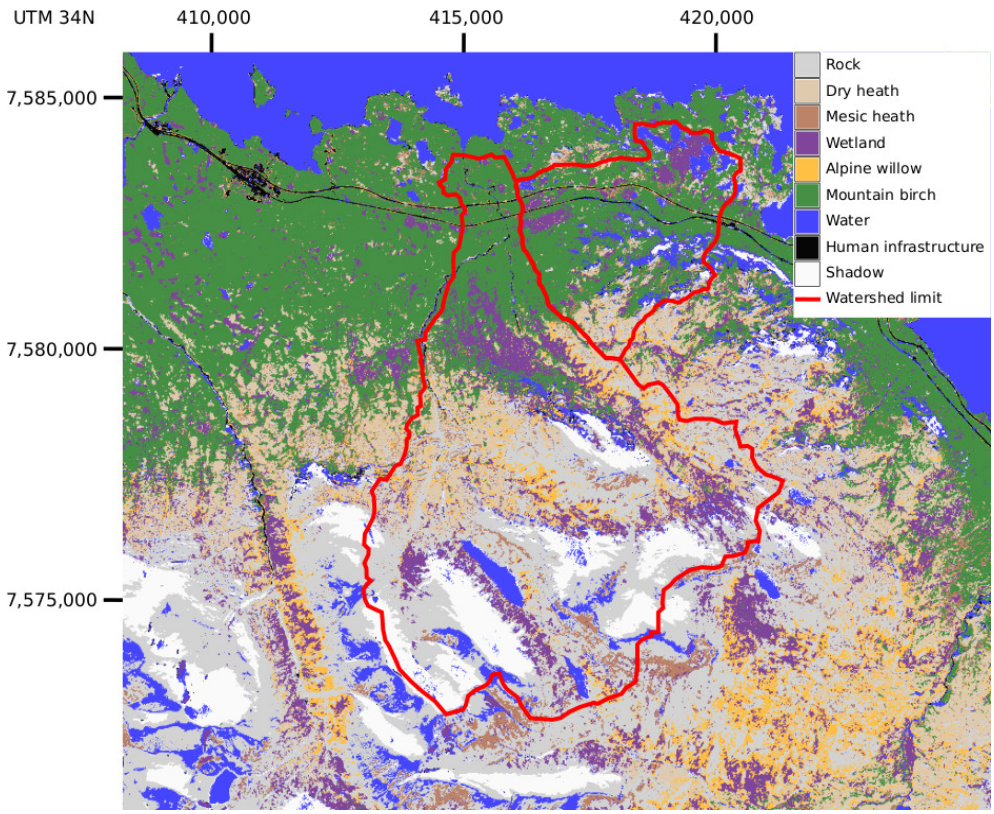

Figure 3. Image classified by support vector machine from the July 2022 field survey.

3.2. Influence of Altitude on Land Cover

The land cover appears to be strongly conditioned by altitude. Altitudinal zonation of land cover is encountered in various arctic contexts [43–45], including in the Abisko region [46,47]. In the Miellajokka catchment, the seasonal variability of the hydrogeochemistry of the stream indicates a strong altitudinal control on hydrological processes, especially during the spring freshet [48], while hydrological conditions strongly interact with vegetation and carbon dioxide fluxes [49]. Table 6, constructed by cross-referencing the land cover map with the ArticDEM, illustrates this phenomenon in the studied watersheds.

Table 6. Percentage of land cover classes according to altitudinal levels. The "Water", "Human infrastructure," and "Shadow" classes are not taken into account.

Land Cover	Level Class (m)			
	Subalpine <600	**Low Alpine [600,800]**	**High Alpine [800,1100]**	**Nival >1100**
Rock	2	5	42	84
Dry heath	3	28	21	1
Mesic heath	3	6	2	10
Wetland	10	16	17	5
Alpine willow	1	7	16	0
Mountain birch	81	38	2	0

The subalpine level at altitudes below 600 m is mainly occupied by the "Mountain birch" class. The Alpine stage includes the "Dry heath," "Mesic heath," "Wetland," and "Alpine willow" formations. It is divided into two sub-stages: Between 600 and 800 m altitude, the "Mountain birch" class is still very present. Above 800 m, this class gives way to the rock class. The nival stage is composed only of rock, probably because it depends on harsher life conditions and more intense erosive processes at higher elevations.

3.3. Comparison between Past and Present Vegetation Maps

Three maps of parts of our study area have been produced by different authors. A map was constructed from aerial images of 8 August 1970 and 29 July 2000 [26], but the area covered is too small to allow comparison with our data. Another map of the Stordalen watershed by Lundin et al. [31] was obtained from images from a helicopter flight on 1 August 2008. The most recent map of the Miellajokka watershed was produced by Reese et al. [18,50] from SPOT5 images of 28 July 2011 and laser data acquired under leaf-on conditions from two scanning dates (20 August 2010 and 9 September 2010). As the semantics of these maps are not identical to ours, an analysis of the variable typologies is necessary prior to the study of the landscape evolution. In order to overlay the maps and then calculate statistics, the Lundin and Reese maps extracted from the publications were georeferenced from control points identified in the landscape.

3.3.1. Comparison with the Map of Reese (Based on Data Acquired in 2010)

Reese et al. [18,50] produced a land cover map with a larger number of classes. In order to compare the Reese map with our data, some classes of the Reese map are merged. "Snow ice" and "Snow bed" classes are grouped together. "Dry heath," "Extremely dry heath," and "Grass heath" are also grouped together. The "Human infrastructure" class is not considered because it does not exist in Reese's study. "Alpine meadow" and "Tall Alpine meadow" were not confirmed by ground observations during our field trip.

The spatial distribution of the classes is slightly different (Table 7). The "Rock" class accounts for 36% of our classification and only 14% for the Reese map.

Table 7. Percentage of land cover classes of Reese and our classification in the Miellajokka watershed. The asterisks (*) indicate classes that were not observed during our field trip.

Class	Reese (2010)	Our Classification
Rock	14	39
Dry heath/Extremely dry heath/Grass heath	26	12
Mesic heath	4	4
Wetland	4	17
Alpine willow	19	7
Mountain birch	13	15
Water	4	6
Snow Ice, Snow bed	5	*
Alpine meadow/Tall alpine meadow	11	*

The change matrix shown in Table 8 encompasses the differences in the semantics of classes and the changes in the landscape between the dates of the two maps (i.e., 2014 and 2022), and there may also be discrepancies due to the use of different methodologies. Three elements can explain these differences. (1) The landscape is natural. There are no parcels to structure it. Between areas occupied by two vegetation classes, there is often a transition zone, which is difficult to assign to a class. (2) The class definition of Reese [18] takes into account the height of the stratum using metrics derived from laser acquisitions, a technology we did not employ. (3) The landscape has evolved between 2010 and 2022.

Table 8. Change matrix comparing our classification to the map of Reese. Each column corresponds to the percentage of pixels of a class obtained by our classification in the function of the Reese map classes. The "Shadow" class is not taken into account.

		Our Classification						
		Rock	**Dry Heath**	**Mesic Heath**	**Wetland**	**Alpine Willow**	**Mountain Birch**	**Water**
Reese map (2010)	Rock	27	3	24	3	2	1	33
	Dry heath/Extremely dry heath/Grass heath	33	41	33	18	33	5	10
	Mesic heath	1	5	3	6	4	11	1
	Wetland	2	5	3	6	9	3	1
	Alpine willow	16	29	20	22	29	12	18
	Mountain birch	0	3	7	18	3	60	2
	Water	3	2	3	4	2	4	23
	Snow Ice, Snow bed	9	1	3	2	1	0	6
	Alpine meadow/Tall alpine meadow	9	11	4	21	17	4	6

Table 8 and Figure 3 shows that some "Rock" areas in the middle of our map are covered by "Grass heath," "Dry heath," and "Alpine willow" on the Reese map. The forest is also growing slightly to the south in sparse patches. On the other hand, "Alpine willow" is also more represented on Reese's map without any conclusion being drawn

because this class is misclassified by Reese [18]: the confusion matrix indicates 20 of 44 pixels are misclassified.

In addition, the "Alpine meadow," which we have not taken into account, is identified as the "Wetland" class on our map (Figure 4), maybe because most of the "Alpine meadow" places were temporarily flooded at the time of observation(see also Section 3.1). This class "Wetland" exists on the map published by Borgelt [50], but it is not present in the confusion matrix published by Reese [18]. The other classes do not show clear differences in their proportion and spatial distribution.

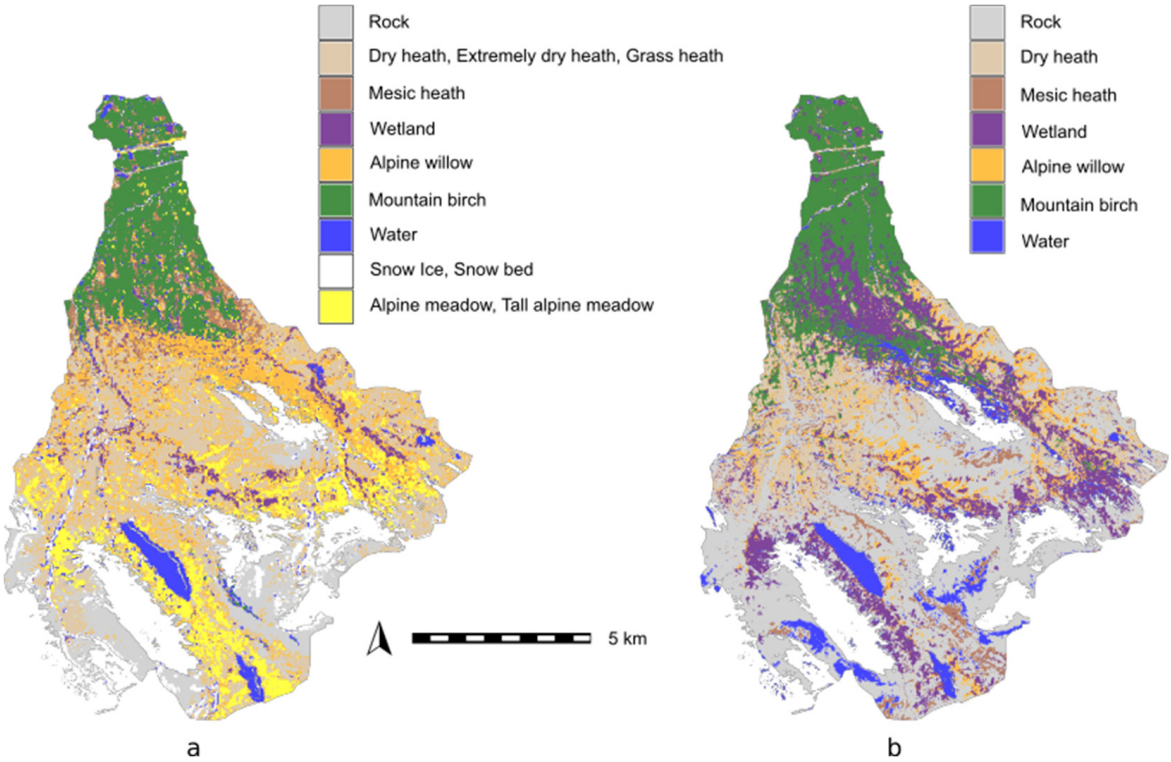

Figure 4. Land cover map by Reese (2010) (**a**) and our reclassified map (2022) (**b**) in the Miellajokka watershed.

3.3.2. Comparison with the Map of Lundin (Based on Data Acquired in 2008)

The definition of classes in Lundin et al. [31] differs from the one presented in this study, with a smaller number of classes in the map of Lundin. So, the classes we used need to be modified to achieve consistency between the two maps. Grouping the "Dry heath," "Mesic heath," and "Alpine willow" classes of our classification allows them to be compared with the "Alpine tundra" class of the map of Lundin. Similarly, our "Wetland" class is compared with the "Peatland" class of the map of Lundin. The classes "Human infrastructure" and "Non-vegetated" correspond to roads, railways, and buildings. The latter class is much more represented on the map of Lundin (Table 9). The differences are related to a larger road and railway footprint, which does not affect the landscape dynamics. This observation shows the satisfactory overlay of these two maps.

The change matrix (Table 10) shows that the "Rock" class is also more represented on the map of Lundin, which covers twice as much space. The areas of this class that are not classified as "Rock" for our map are located in the south of the map (Figure 5). They are contiguous to the "Rock" areas of our map. It is also possible that there has been a forest expansion between 2008 and 2002 in this area. Indeed, the forest has grown between 2008 and 2022. It has gained some space in all land cover categories. Furthermore, some areas of "Peatland" appear to be transformed into "Wetland" but Lundin et al. [31] indicate "Peatlands" were subdivided into wet areas (fen) and dry areas (bog) proportionally to

what was found by Malmer et al. (2005)". It is, therefore, not possible to draw a conclusion from this observation. In summary, it is possible to compare our map with the map of Lundin after a semantic analysis of the categories. The main differences between the two maps concern the south of the Stordalen watershed, where the Alpine tundra and forest are intermixed, as shown on the discrepancies map (Figure 5c). The forest seems to have taken over areas previously occupied by tundra.

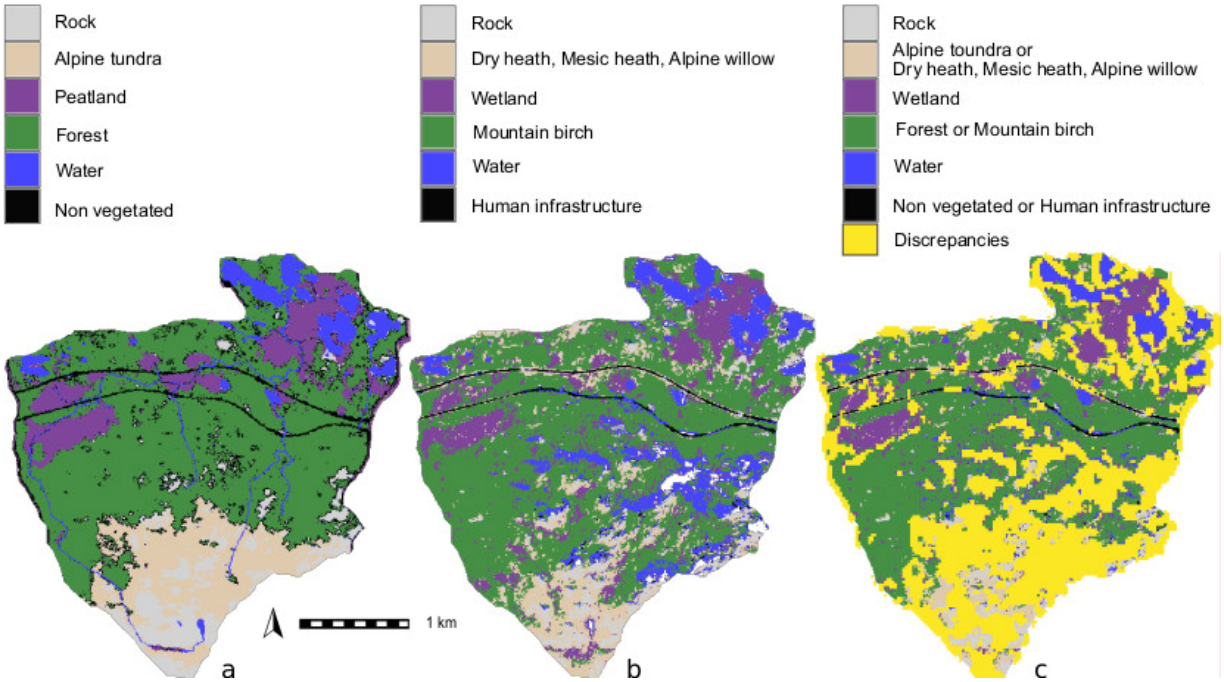

Figure 5. Land cover map by Lundin (2008) (**a**) and our reclassified map (2022) (**b**) in the Stordalen watershed. (**c**) Discrepancies between the two maps.

Table 9. Percentage of land cover classes of the map of Lundin in the Stordalen watershed. In our classification, the "Alpine tundra" class corresponds to the grouping of classes "Dry heath," "Mesic heath," and "Alpine willow." The class "Peatland" corresponds to "Wetland". The class "Non-vegetated" corresponds to "Human infrastructure".

Class	Lundin (2008)	Our Classification
Rock	9	5
Alpine tundra	13	12
Peatland	11	15
Forest	51	54
Water	7	12
Non-vegetated	9	2

Table 10. Change matrix comparing our classification (2022) to the map of Lundin (2008). Each column corresponds to the percentage of pixels of a class obtained by our classification in the function of the classes of the Lundin map. The shadow class is not taken into account.

		Our Classification					
		Rock	**Dry Heath Mesic Heath Alpine Willow**	**Wetland**	**Mountain Birch**	**Water**	**Human infrastructure**
Lundin map (2008)	Rock	41	30	5	3	5	4
	Alpine tundra	27	27	9	10	10	7
	Peatland	3	6	40	6	5	6
	Forest	15	24	33	69	45	27
	Water	4	3	7	4	26	4
	Non-vegetated	10	10	6	8	9	52

4. Discussion

The methodology implemented in this study requires little sampling effort to quickly obtain a land cover map. This operation is feasible every year to monitor the evolution of land cover. These results are particularly important in a region subject to climate change, which is currently undergoing major upheaval.

The results of the Sentinel-2 image classification show a structuring of the landscape as a function of elevation, with vegetation levels changing with altitude [51]. In the Miellajokka and Stordalen catchments, three levels are present. The sub-alpine level (<600 m) is mainly occupied by birch forests. The alpine level [600 m, 1100 m] is characterized by heath and willow. This level could be split into two sub-levels according to the respective abundance of birch forests at lower altitudes and outcrops at upper altitudes. The upper level, the nival level (>1100 m), is only composed of rock. Some temporary open water bodies were localized at high altitudes, which is a surprising feature that may be linked to the late melt in high-elevation snow bodies.

Comparison between past and present vegetation maps is not straightforward due to a lack of common typology field survey protocols. Nevertheless, it was possible to identify a change in the landscape between 2008 and 2022. Comparative analysis of the maps of Lundin [31] and Reese [18] with the one presented in this study demonstrated an extension of the forest on the tundra towards the south (i.e., toward higher elevations) during the 2008–2022 period. This finding is in agreement with Rundqvist's study [52], which shows an upward movement in the species observed over a study period between 1976 and 2010. Nevertheless, one should be careful with this possible interpretation because of the statistical uncertainty of these different classifications. This trend could be a consequence of the ongoing climate warming demonstrated across the Arctic [53,54].

5. Conclusions

In this study, we provided a new land cover map for two watersheds located nearby the Abisko Scientific Research Station, to be used in future permafrost modeling studies in the framework of the HiPerBorea project (hiperborea.omp.eu) using the permaFoam cryohydrogeological simulator [16,28]. This new map also provides some insights into recent land cover changes in the studied area by comparison with previous maps based on data acquired in 2008 [31] and 2010 [18]. High-elevation temporary water bodies have been detected, which requires further investigation in the future.

The proximity of the Abisko observation station makes the Miellajokka and Stordalen watersheds a privileged study area for the evolution of landscapes in the Arctic zone, in

particular, where thawing of the permafrost at high altitudes is attested. This monitoring requires annual surveys according to a unified protocol in terms of sampling, definition of classes, and method of recording in order to monitor the evolution of this region under ongoing climate change. The present study presents a protocol that would be suitable for such a purpose.

At the same time, the study of land cover in the Arctic zone poses a number of difficulties. The areas are covered by snow for a large part of the year, which limits observations to a few months of summer. Acquisition by passive optical satellites can only be made during the period with daylight. Fortunately, this period includes the summer months when snow cover is at its minimum extension. Cloud cover frequently hampers optical acquisitions. For the year 2022, only one Sentinel-2 image could be used, which illustrates the problems of relying on optical images only in such environments. Future studies could involve radar images whose acquisition is not affected by clouds and polar night.

Author Contributions: Conceptualization, Y.A. and L.O.; methodology, Y.A. and L.O.; software, Y.A.; validation, Y.A., E.J.L., J.G., O.S.P., S.C. and L.O.; writing—original draft preparation, Y.A. and L.O.; investigation, Y.A., L.O. and S.C.; writing—review and editing, Y.A., E.J.L., J.G., O.S.P., S.C. and L.O.; project administration, L.O.; funding acquisition, L.O. All authors have read and agreed to the published version of the manuscript.

Funding: This study has been funded by the French Research Agency ANR (grant n ◦ ANR-19 CE46-0003-01), O.S. Pokrovsky was partially supported by the TSU Development Programme "Priority-2030".

Data Availability Statement: The produced map and field data are available upon request to the corresponding author.

Acknowledgments: The authors would like to thank Reiner Giesler and Emily Pickering Pedersen for their help in preparing the fieldwork.

Conflicts of Interest: The authors declare no conflict of interest.

References

1. Walvoord, M.; Kurylyk, B. Hydrologic Impacts of Thawing Permafrost—A Review. *Vadose Zone J.* **2016**, *15*, 6. [CrossRef]
2. Meyer, G.; Humphreys, E.R.; Melton, J.R.; Cannon, A.J.; Lafleur, P.M. Simulating shrubs and their energy and carbon dioxide fluxes in Canada's Low Arctic with the Canadian Land Surface Scheme Including Biogeochemical Cycles (CLASSIC). *Biogeosciences* **2021**, *18*, 3263–3283. [CrossRef]
3. Jones, B.J.; Grosse, G.; Farquharson, L.M.; Roy-Léveillée, P.; Veremeeva, A.; Kanevskiy, M.Z.; Gaglioti, B.V.; Breen, A.L.; Parsekian, A.D.; Ulrich, M.; et al. Lake and drained lake basin systems in lowland permafrost regions. *Nat. Rev. Earth Environ.* **2022**, *3*, 85–98. [CrossRef]
4. Cable, W.L.; Romanovsky, V.E.; Jorgenson, M.T. Scaling-up permafrost thermal measurements in western Alaska using an ecotype approach. *Cryosphere* **2016**, *10*, 2517–2532. [CrossRef]
5. Douglas, T.A.; Zhang, C. Machine learning analyses of remote sensing measurements establish strong relationships between vegetation and snow depth in the boreal forest of Interior Alaska. *Environ. Res. Lett.* **2021**, *16*, 065014. [CrossRef]
6. Zhang, Y.; Lantz, T.C.; Touzi, R.; Feng, W.; Kokelj, S.V. Landscape-scale variations in near-surface soil temperature and active-layer thickness: Implications for high-resolution permafrost mapping. *Permafr. Periglac Process* **2021**, *32*, 627–640. [CrossRef]
7. Heijmans, M.M.P.D.; Magnússon, R.Í.; Lara, M.J.; Frost, G.V.; Myers-Smith, I.; van Huissteden, J.; Jorgenson, M.T.; Fedorov, A.N.; Epstein, H.E.; Lawrence, D.M.; et al. Tundra vegetation change and impacts on permafrost. *Nat. Rev. Earth Environ.* **2022**, *3*, 68–84. [CrossRef]
8. Bagard, M.-L.; Schmitt, A.-D.; Chabaux, F.; Pokrovsky, O.S.; Viers, J.; Stille, P.; Labolle, F.; Prokushkin, A. Biogeochemistry of stable Ca and radiogenic Sr isotopes in a larch-covered permafrost-dominated watershed of Central Siberia. *Geochim. Et Cosmochim. Acta* **2013**, *114*, 169–187. [CrossRef]
9. Oehri, J.; Schaepman-Strub, G.; Kim, J.-S.; Grysko, R.; Kropp, H.; Grünberg, I.; Zemlianskii, V.; Sonnentag, O.; Euskirchen, E.S.; Reji Chacko, M.; et al. Vegetation type is an important predictor of the arctic summer land surface energy budget. *Nat. Commun.* **2022**, *13*, 6379. [CrossRef]
10. Lenoir, J.; Graae, B.J.; Aarrestad, P.A.; Alsos, I.G.; Armbruster, W.S.; Austrheim, G.; Bergendorff, C.; Birks, H.J.B.; Bråthen, K.A.; Brunet, J.; et al. Local temperatures inferred from plant communities suggest strong spatial buffering of climate warming across Northern Europe. *Glob. Chang. Biol.* **2013**, *19*, 1470–1481. [CrossRef]
11. Aalto, J.; Scherrer, D.; Lenoir, J.; Guisan, A.; Luoto, M. Biogeophysical controls on soil-atmosphere thermal differences: Implications on warming Arctic ecosystems. *Environ. Res. Lett.* **2018**, *13*, 7. [CrossRef]

12. De Frenne, P.; Zellweger, F.; Rodríguez-Sánchez, F.; Scheffers, B.R.; Hylander, K.; Luoto, M.; Vellend, M.; Verheyen, K.; Lenoir, J. Global buffering of temperatures under forest canopies. *Nat. Ecol. Evol.* **2019**, *3*, 744–749. [CrossRef]
13. Stuenzi, S.M.; Boike, J.; Gädeke, A.; Herzschuh, U.; Krise, S.; Pestryakova, A.; Westermann, S.; Langer, M. Sensitivity of ecosystem-protected permafrost under changing boreal forest structures. *Environ. Res. Lett.* **2021**, *16*, 8. [CrossRef]
14. Stuenzi, S.M.; Boike, J.; Cable, W.; Herzschuh, U.; Kruse, S.; Pestryakova, L.A.; von Deimling, T.S.; Westermann, S.; Zakharov, E.S.; Langer, M. Variability of the surface energy balance in permafrost-underlain boreal forest. *Biogeosciences* **2021**, *18*, 343–365. [CrossRef]
15. Park, H.; Yamazaki, T.; Yamamoto, K.; Ohta, T. Tempo-spatial characteristics of energy budget and evapotranspiration in the Eastern Siberia. *Agric. For. Meteorol.* **2018**, *148*, 1990–2005. [CrossRef]
16. Orgogozo, L.; Prokushkin, A.S.; Pokrovsky, O.S.; Grenier, C.; Quintard, M.; Viers, J.; Audry, S. Water and energy transfer modeling in a permafrost-dominated, forested catchment of Central Siberia: The key rôle of rooting depth. *Permafr. Periglac. Process.* **2019**, *30*, 75–89. [CrossRef]
17. Bartsch, A.; Höfler, A.; Kroisleitner, C.; Trofaier, A.M. Land Cover Mapping in Northern High Latitude Permafrost Regions with Satellite Data: Achievements and Remaining Challenges. *Remote Sens.* **2016**, *8*, 979. [CrossRef]
18. Reese, H.; Nyström, M.; Nordkvist, K.; Olsson, H. Combining airborne laser scanning data and optical satellite data for classification of alpine vegetation. *Int. J. Appl. Earth Obs. Geoinf.* **2014**, *27*, 81–90. [CrossRef]
19. Greaves, H.E.; Eitel, J.U.H.; Vierling, L.A.; Boelman, N.T.; Griffin, K.L.; Magney, T.S.; Prager, C.M. 20 cm resolution mapping of tundra vegetation communities provides an ecological baseline for important research areas in a changing Arctic environment. *Environ. Res. Commun.* **2019**, *1*, 105004. [CrossRef]
20. Langford, Z.L.; Kumar, J.; Hoffman, F.M.; Breen, A.L.; Iversen, C.M. Arctic Vegetation Mapping Using Unsupervised Training Datasets and Convolutional Neural Networks. *Remote Sens.* **2019**, *11*, 69. [CrossRef]
21. Beamish, A.; Raynolds, M.K.; Epstein, H.; Frost, G.V.; Macander, M.J.; Bergstedt, H.; Bartsch, A.; Kruse, S.; Miles, V.; Tanis, C.M.; et al. Recent trends and remaining challenges for optical remote sensing of Arctic tundra vegetation: A review and outlook. *Remote Sens. Environ.* **2020**, *246*, 111872. [CrossRef]
22. Rudd, D.A.; Karami, M.; Fensholt, R. Towards High-Resolution Land-Cover Classification of Greenland: A Case Study Covering Kobbefjord, Disko and Zackenberg. *Remote Sens.* **2021**, *13*, 3559. [CrossRef]
23. IPCC. Summary for Policymakers. In *IPCC Special Report on the Ocean and Cryosphere in a Changing Climate*; Pörtner, H.-O., Roberts, D.C., Masson-Delmotte, V., Zhai, P., Tignor, M., Poloczanska, E., Mintenbeck, K., Nicolai, M., Okem, A., Petzold, J., et al., Eds.; IPCC: Geneva, Switzerland, 2019; Available online: https://www.ipcc.ch/site/assets/uploads/sites/3/2019/12/SROCC_FullReport_FINAL.pdf (accessed on 12 April 2023).
24. Patzner, M.S.; Logan, M.; McKenna, A.M.; Young, R.B.; Zhou, Z.; Joss, H.; Mueller, C.W.; Carmen, H.; Scholten, T.; Straub, D.; et al. Microbial iron cycling during palsa hillslope collapse promotes greenhouse gas emissions before complete permafrost thaw. *Commun. Earth Environ.* **2022**, *3*, 76. [CrossRef]
25. Loranty, M.L.; Abbott, B.W.; Blok, D.; Douglas, T.A.; Epstein, H.E.; Forbes, B.C.; Jones, B.M.; Kholodov, A.L.; Kropp, H.; Malhotra, A.; et al. Reviews and syntheses: Changing ecosystem influences on soil thermal regimes in northern high-latitude permafrost regions. *Biogeosciences* **2018**, *15*, 5287–5313. [CrossRef]
26. Malmer, N.; Johansson, T.; Olsrud, M.; Christensen, T.R. Vegetation, climatic changes and net carbon sequestration in a North-Scandinavian subarctic mire over 30 years. *Glob. Chang. Biol.* **2005**, *11*, 1895–1909. [CrossRef]
27. Tang, J.; Miller, P.A.; Persson, A.; Olefeldt, D.; Pilesjö, P.; Heliasz, M.; Jackowicz-Korczynski, M.; Yang, Z.; Smith, B.; Callaghan, T.V.; et al. Carbon budget estimation of a subarctic catchment using a dynamic ecosystem model at high spatial resolution. *Biogeosciences* **2015**, *12*, 2791–2808. [CrossRef]
28. Orgogozo, L.; Xavier, T.; Oulbani, H.; Grenier, C. Permafrost modelling with OpenFOAM®: New advancements of the permaFoam solver. *Comput. Phys. Commun.* **2023**, *282*, 108541. [CrossRef]
29. Giesler, R.; Lyon, S.W.; Mörth, C.-M.; Karlsson, J.; Karlsson, E.M.; Jantze, E.J.; Destouni, G.; Humborg, C. Catchment-scale dissolved carbon concentrations and export estimates across six subarctic streams in northern Sweden. *Biogeosciences* **2014**, *11*, 525–537. [CrossRef]
30. Lundin, E.J.; Giesler, R.; Persson, A.; Thompson, M.S.; Karlsson, J. Integrating carbon emissions from lakes and streams in a subarctic catchment. *JGR Biogeosci.* **2013**, *118*, 1200–1207. [CrossRef]
31. Lundin, E.J.; Klaminder, J.; Giesler, R.; Persson, A.; Olefeldt, D.; Heliasz, M.; Christensen, T.R.; Karlsson, J. Is the subarctic landscape still a carbon sink? Evidence from a detailed catchment balance. *Geophys. Res. Lett.* **2016**, *43*, 1988–1995. [CrossRef]
32. Mzobe, P.; Berggren, M.; Pilesjö, P.; Lundin, E.; Olefeldt, D.; Roulet, N.T.; Persson, A. Dissolved organic carbon in streams within a subarctic catchment analysed using a GIS/remote sensing approach. *PLoS ONE* **2018**, *13*, e0199608. [CrossRef] [PubMed]
33. Mzobe, P.; Yan, Y.; Berggren, M.; Roulet, N.T.; Persson, A. Morphometric Control on Dissolved Organic Carbon in Subarctic Streams. *J. Geophys. Res. Biogeosci.* **2020**, *125*, e2019JG005348. [CrossRef]
34. Hardisky, M.A.; Kiemas, V.; Daiber, F.C. Remote sensing salt marsh biomass and stress detection. *Adv. Space Res.* **1983**, *2*, 219–229. [CrossRef]
35. Gao, B.C. NDWI—A normalized difference water index for remote sensing of vegetation for liquid water from space. *Remote Sens. Environ.* **1996**, *58*, 257–266. [CrossRef]

36. Ostadabbas, H.; Weippert, H.; Behr, F.J. Using the synergy of qfield for collecting data on-site and qgis for interactive map creation by alkis® data extraction and implementation in postgresql for urban planning processes. *Int. Arch. Photogramm. Remote Sens. Spatial Inf. Sci.* **2020**, 679–683. [CrossRef]
37. Avci, C.; Budak, M.; Yagmur, N.; Balcik, F.B. Comparison between random forest and support vector machine algorithms for LULC classification. *Int. J. Eng. Geosci.* **2023**, *8*, 1–10. [CrossRef]
38. Mountrakis, G.; Im, J.; Ogole, C. Support vector machies in remote sensing: A review. *ISPRS J. Photogramm.* **2011**, *66*, 247–259. [CrossRef]
39. Pal, M.; Mather, P.M. Support vector machines for classification in remote sensing. *Int. J. Remote Sens.* **2005**, *26*, 1007–1011. [CrossRef]
40. Breiman, L. Statistical Modeling: The Two Cultures. *Stat. Sci.* **2001**, *16*, 199–231. [CrossRef]
41. Belgiu, M.; Dragut, L. Random forest in remote sensing: A review of applications and future directions. *ISPRS J. Photogramm. Remote Sens.* **2016**, *114*, 24–31. [CrossRef]
42. Neteler, M.; Mitasova, H. *Open Source GIS: A GRASS GIS Approach*, 3rd ed.; Springer: New York, NY, USA, 2008.
43. Ermakov, N.; Shaulo, D.; Maltseva, T. The class Mulgedio-Aconitetea in Siberia. *Phytocoenologia* **2000**, *30*, 145–192. [CrossRef]
44. Hjort, J.; Luoto, M. Interaction of geomorphic and ecologic features across altitudinal zones in a subarctic landscape. *Geomorphology* **2009**, *112*, 324–333. [CrossRef]
45. Sieg, B.; Drees, B.; Hasse, T. High-altitude vegetation of continental West Greenland. *Phytocoenologia* **2009**, *39*, 27–50. [CrossRef]
46. Sundqvist, M.; Giesler, R.; Graae, B.J.; Wallander, H.; Fogelberg, E.; Wardle, D.A. Interactive effects of vegetation type and elevation on aboveground and belowground properties in a subarctic tundra. *Oikos* **2011**, *120*, 128–142. [CrossRef]
47. Sundqvist, M.; Liu, Z.; Giesler, R.; Wardle, D.A. Plant and microbial responses to nitrogen and phosphorus addition across an elevational gradient in subarctic tundra. *Ecology* **2014**, *95*, 1819–1835. [CrossRef]
48. Lyon, S.W.; Ploum, S.W.; van der Velde, Y.; Rocher-Ros, G.; Mörth, C.-M.; Giesler, R. Lessons learned from monitoring the stable water isotopic variability in precipitation and streamflow across a snow-dominated subarctic catchment. *Arct. Antarct. Alp. Res.* **2018**, *50*, e1454778. [CrossRef]
49. Rocher-Ros, G.; Sponseller, R.A.; Lidberg, W.; Mörth, C.-M.; Giesler, R. Landscape process domains drive patterns of CO2 evasion from river networks. *Limnol. Oceanogr. Lett.* **2019**, *4*, 87–95. [CrossRef]
50. Borgelt, J. Terrestrial Respiration across Tundra Vegetation Types—Implications for Arctic Carbon Modelling. Master's Thesis, Umeå University, Umeå, Sweden, 2017.
51. Troll, C. High mountain belts between the polar caps and the equator: Their definition and lower limit. *Arct. Alp. Res.* **1973**, *5*, A19–A27.
52. Rundqvist, S.; Hedenås, H.; Sandström, A.; Emanuelsson, U.; Eriksson, H.; Jonasson, C.; Callaghan, T.V. Tree and Shrub Expansion Over the Past 34 Years at the Tree-Line Near Abisko, Sweden. *AMBIO* **2011**, *40*, 683–692. [CrossRef]
53. Rees, W.G.; Hofgaard, A.; Boudreau, S.; Cairns, D.M.; Harper, K.; Mamet, S.; Mathisen, I.; Swirad, Z.; Tutubalina, O. Is subarctic forest advance able to keep pace with climate change? *Glob. Chang. Biol.* **2020**, *26*, 3965–3977. [CrossRef]
54. Berner, L.T.; Goetz, S.J. Satellite observations document trends consistent with a boreal forest biome shift. *Glob. Chang. Biol.* **2022**, *28*, 3275–3292. [CrossRef] [PubMed]

Disclaimer/Publisher's Note: The statements, opinions and data contained in all publications are solely those of the individual author(s) and contributor(s) and not of MDPI and/or the editor(s). MDPI and/or the editor(s) disclaim responsibility for any injury to people or property resulting from any ideas, methods, instructions or products referred to in the content.